Gene silencing in *Cryptosporidium*: A rapid approach to identify novel targets for drug development.

Castellanos-Gonzalez A*[1], Martinez-Traverso G[1], Fishbeck K, Nava S[1], White AC Jr[1]. Infectious Disease Division, Department of Internal Medicine, University of Texas Medical Branch, Galveston Tx[1]

***Address correspondence to:**
Alejandro Castellanos-Gonzalez
Infectious Disease Division
Department of Internal Medicine
University of Texas Medical Branch
301 University Boulevard, Route 0435
Galveston, TX 77555-0435
Email alcastel@utmb.edu

Key words: *Cryptosporidium*, Cryptosporidiosis, Gene silencing, Ellagic Acid

Abstract:

Background: Cryptosporidiosis is a major cause of diarrheal disease. However, the only drug approved for cryptosporidiosis does not work well in high risk populations. Therefore, novel drugs are urgently needed. Then, the identification of novel is necessary to develop new therapies against this parasite. Recently, we have developed a rapid method to block gene expression in *Cryptosporidium* by using pre-assembled complexes of *Cryptosporidium* antisense RNA and human protein with slicer activity (Argonaute 2). We hypothesized that structural proteins, proteases, enzymes nucleotide synthesis and transcription factors are essential for parasite development, thus in this work we knock down expression of 4 selected genes: Actin, Apicomplexan DNA-binding protein (AP2), Rhomboid protein 1 (Rom 1) and nucleoside diphosphate kinase (NDK) and elucidated its role during invasion, proliferation and egress of *Cryptosporidium*.

Methods: We used protein transfection reagents (PTR) to introduce pre-assembled complexes of antisense RNA and human Argonaute 2 into *Cryptosporidium parvum* oocysts, the complexes blocked expression of Actin (Act), Transcription factor AP2 (AP2), nucleoside diphosphate kinase (DKN), and rhomboid protein 1 (Rom1). After gene silencing, we evaluated parasite reduction using *In vitro* models of excystation, invasion, proliferation and egress. We evaluated the potency of ellagic acid, a nucleoside diphosphate kinase inhibitor for anti-cryptosporidial activity using a model of *in vitro* infection with human HCT-8 cells.

Results: Silencing of Act, AP2, NDK and Rom1 reduce significantly invasion, proliferation and egress of *Cryptosporidium*. We showed that silencing of NDK markedly inhibited *Cryptosporidium* proliferation. This was confirmed by demonstration that ellagic acid reduced the number of parasites at micro molar concentrations (EC 50 =15-30 μM) without showing any toxic effect on human cells.

Conclusions: Overall the results confirmed the usefulness RNA silencing can be used to identify novel targets for drug development against *Cryptosporidium*. We identified ellagic acid (EA), a nucleoside diphosphate kinase inhibitor also blocks *Cryptosporidium* proliferation. Since EA is a dietary supplement approved for human use, then this compound should be studied as a potential treatment for cryptosporidiosis.

Author summary

The World Health Organization reports diarrhea kills around 760,000 children under five every year. *Cryptosporidium* infection is a leading cause of diarrhea morbidity and mortality. Current therapies to treat this infection are suboptimal, therefore novel treatments are urgently needed. We used genetic tools to identify novel targets for drug development, thus in this work we evaluated the role of 4 genes during *Cryptosporidium* infection. We demonstrated that silencing of nucleoside-diphosphate kinase (NDK) drastically reduced invasion, proliferation and egress of this parasite. To validate these finding we used the Ellagic acid (EA) an inhibitor of NDK to treat infected intestinal cells. Our results confirmed that the EA blocks parasite proliferation on infected cells. Interestingly we observed that the ellagic acid also has anti cryptosporidial activity by inducing apoptosis. Since EA is a dietary supplement already approved for human use, then this compound has potential to be used as a rapid alternative to treat Cryptosporidiosis.

Introduction

Cryptosporidium is a leading cause of moderate-to-severe diarrhea in children under two years old and the leading pathogen associated with death in toddlers (ages 12 to 23 months[1]). Nitazoxanide is only one FDA approved medicine available for cryptosporidiosis, but it has limited efficacy in the population at the highest risk for poor outcomes. There is a strong consensus that better treatment options are urgently needed[2-4]. The limitation of tools to genetically manipulate gene expression in this parasite has been identified as a major hurdle for drug and vaccine development[2,4]. We developed a method to silence genes in this parasite by using preassembled complexes of *Cryptosporidium* single strand RNA and the human enzyme Argonaute 2 (hAgo2)[5]. We hypothesized that this method could be used to study key steps of infection and identify novel targets for drug and vaccine development. In the present work we

used gene silencing to evaluate the role of Actin (Act), Rhomboid protein 1 (Rom1), transcription factor AP2 (AP2) and Nucleoside diphosphate kinase (NDK) 1 during *Cryptosporidium* infection.

Methods.

Target selection for silencing experiments.

Initially, we selected 100 genes for silencing experiments (Table S1), for these experiments mRNA sequences were obtained from CryptoDB (https://cryptodb.org/) and Gene Bank data bases (https://www.ncbi.nlm.nih.gov/nucleotide/). Selected genes codes for: structural proteins, transcription factors, kinases and proteases (Table S1). In these experiments we observed silencing ranging from 30-94%, however in this study we only analyzed genes that were silenced >75% (Table 1, figure 1).

Antisense ssRNA design.

Antisense single stranded RNA (ssRNA) used in silencing experiments was designed by using the computational software sFold 2.2 (http://sfold.wadsworth.org). We used as template the full sequences of mRNA targets (accession numbers in table S1), initially we generated all possible ssRNA antisense sequences of 21 nucleotides for each target, however we only selected optimal ssRNAs based in sFold ranking, these scores reflects parameters such as, local free energy and binding probability (C-G>40%). We synthetized selected ssRNAs from a commercial vendor (Integrated DNA Technologies, Coralville, IA), for silencing experiments the ssRNA was modified as follow: 21 nt ssRNA was capped with a phosphorylation at 5' end and was modified with a deoxinucleotide (dTdT) tail at 3' end (Table S2). Scrambled control ssRNA (Table S2) was designed using siRNA wizard software (Invivogen, San Diego CA).

Gene silencing in C. parvum oocysts.

For transfection experiments, we used oocysts (Iowa isolate) purchased from University of Arizona (Sterling Laboratories, Tucson, AZ). First the oocyst were prepared for transfection: the oocysts ($1x10^6$ for each target) were transferred to 1.5 ml tubes, the samples were diluted with nuclease free water (Fisher Scientific, Hampton, NH) and then centrifuged for 10 minutes at a speed of 8,000 rpm (using microcentrifuge Eppendorf 5424). The supernatant was discarded and then the pellet was resuspended with 20 µl of nuclease-free water and then the tubes with the sample were placed at RT before adding transfection reagents. To assemble silencer complexes, first the ssRNAs were diluted with water at 100 nM, then samples were heated for 1 minute at 95°C and placed on ice. Complexes of ssRNA-hAgo2 were assembled in 1.5 ml microcentrifuge tubes, each tube contained 2.5 µl of diluted ssRNA 100 nM, 2.5 µl [62.5 ng/ul] of human Argonaute 2 (hAgo2) protein (Sino Biologicals, North Wales, PA) and 15 µl of Assembling Buffer [2 mM $Mg(OAc)_2$, 150 mM KOHAc, 30 mM HEPES, 5 mM DTT, nuclease-free water]. The mixture was incubated for 1 hour at RT. After incubation, the complexes were encapsulated by adding 15 µl of protein transfection reagent (PTR) Pro-Ject ™ (Thermo Scientific, Rockford, IL). The sample was mixed by pipetting and then incubated for 30 min, at RT. For transfection experiments the encapsulated complexes were added to oocysts and incubated at room temperature for 2 hrs. The slicer activity of hAgo2 was activated by incubating at 37 °C for 2 hrs. The reaction was stopped by adding 350 µl RLT lysis buffer (RNeasy kit, Qiagen, Hilden, Germany) and then samples were stored at -20°C for its posterior analysis by RT-PCR. For some experiments we used only PTR or PTR with unrelated ssRNAs, scrambled ssRNA (Table S2).

RNA extraction and evaluation of silencing by RT-PCR

Prior to RNA isolation, samples (previously stored at -20°C) were thawed at 95°C for 2 minutes. Then, the total RNA was extracted from samples with the Qiagen's RNeasy Plus Mini Kit

(Qiagen, Valencia CA) following the instructions of the vendor. The RNA was eluted from purification columns with 100 µl of RNase-free water, then the concentration of eluted RNA was determined by spectrophotometry using a NanoDrop 100 Spectrophotometer (Thermo Fisher Scientific, Waltham MA). The silencing in transfected oocysts was analyzed by qRT-PCR using qScript™ One-Step SYBR® Green qRT-PCR Kit, Low ROX™ (Quanta BioSciences/VWR, Radnor, PA). For RT-PCR experiments, reactions were assembled as follow: 2 µl of purified RNA template [20 ng/µl], 5 µl of the One-Step SYBR Green Master Mix, 0.25 µl of each primer at a 10 µM concentration, 0.25 µl of the qScript One-Step reverse transcriptase, and 4.25 µl of nuclease-free water for a total of 10 µl of mix per sample. The RT-PCR mixture (total volume 12 µl) was transferred to 96-well Reaction Plates (0.1 mL) (Applied Biosystems, Foster City, CA) and then RT-PCR amplification was conducted on a 7500 Fast Real-Time PCR System (Applied Biosystems, Foster City, CA) with the following cycling conditions: 50°C for 15 minutes, 95°C for 5 minutes, then 50 cycles of 95°C for 15 seconds and 63°C for 1 minute, followed by a melting point analysis (95°C for 15 seconds, 60°C for 1 minute, 95°C for 15 seconds and 60°C for 15 seconds). Before fold change analysis all the target Ct values for each silenced target were normalized against the *Cryptosporidium* GAPDH. To calculate fold changes between control samples and silenced samples, we used the ΔΔCt method. Results are shown by the average for each target with the respective standard deviation. List of primers used for RT-PCR is indicated in table S3.

Oocyst excystation assays.

Excystation of transfected oocysts was induced with acidic water and taurocholic acid as described before. Briefly, *Cryptosporidium* oocysts were pelleted by centrifugation (500 g), supernatant was discarded and then parasites were resuspended in 25 µl acidic water (pH 2.5), and incubated for 10 minutes on ice. Then, excystation media 250 µl (RPMI-1640 media, 1X

antibiotic/antimycotic solution and 0.8% taurocholic acid sodium salt hydrate] was added. The sample was incubated for 1 hour at 37°C. After excystation we evaluate excystation rate, then the sporozoites were stained with the vital dye carboxyfluorescein succinimidyl ester (CFSE) (CellTraceTM, Thermo Fischer Scientific, Waltham, MA) by adding 2 µM of CFSE and incubating in the dark at 37°C for 15. After staining, the sporozoites were separated from unhatched oocysts by filtration using 3.0 µm nitrocellulose membranes (Merck Millipore Ltd., County Cork, Ireland). Fluorescence of filtered samples was evaluated, for these experiments 200 µl of each filtered sample was transferred to a 96-well plates (Costar, Corning, NY) and then fluorescence was measured with a microplate reader, (FLUOstar Omega, Ortenberg, Germany).

HCT8 cell culture

For infection experiments we used ileocecal cells (HCT-8 cells, ATCC, Manassas, VA). For these experiments cells were thawed at 37°C and then resuspended with 500µl of RPMI-1640 media (Gibco/Thermo Fisher Scientific, Waltham, MA) supplemented with 10% fetal bovine serum (FBS) (Stemcell Technologies, Vancouver, Canada) and 1X antibiotic/antimycotic solution (Gibco/Thermo Fisher Scientific, Waltham, MA) and plated in a 24-well plate (Costar, Corning, NY). Cells were incubated at 37°C overnight.

In vitro Invasion assay.

For invasion assay HCT8 cells were cultured as described. Before the infection, transfected parasites were stained and excysted as described. After filtering, approximately $5x10^5$ (suspended in 250 µl) were added to HCT-8 cells for 1 hr at 37°C. To quantify sporozoites that did not invade cells, 250 µl of the supernatant was collected after incubation and fixed with 50 µl of 4.2%paraformaldehyde solution (Cytofix/Cytoperm, BD BioSciences, San Jose CA). To

quantify sporozoites adhered to the cells, the monolayers were trypsinized by adding 150 µl of 0.25% trypsin-EDTA (Gibco/Thermo Fisher Scientific, Waltham, MA), and incubating at 37°C for 15 minutes. Then, the trypsin was inactivated by adding 500 µl of RPMI media supplemented with 10% FBS. Samples were transferred to 1.5 ml tubes and then centrifuged 10 min at 500 g, supernatant was removed, and pellet was resuspended in 50 µl of Cytofix solution. Fixed sample was resuspended in 200 µl of 1X PBS (Fisher Scientific, Fair Lawn, NJ) and was filtered using a 5 ml Falcon polystyrene round-bottom tube with a cell-strainer cap with a 35 µm nylon mesh (Corning Inc., Corning, NY). Filtered samples were analyzed by flow cytometry using a SE500 Flow Cytometer (Stratedigm, San Jose CA). To define sporozoites populations on infected cells, we analyzed filtered sporozoites stained with CFSE but without HCT-8 cells (Fig 1A).

In vitro Proliferation assay.

The vital dye, CFSE (Thermo Fisher Scientific, Waltham, MA) was used to track proliferation tracker of intracellular stages of *C. parvum*. CFSE is activated by viable cells. However, with each cycle of cell division, the fluorescent intensity decreases. Thus, proliferation was evaluated by measuring the reduction of fluorescence intensity by flow cytometry after 16 hours (Fig 3A and 3B). For these experiments the parasites were silenced (or not) and excysted as described before. After excystation, sporozoites were used to infect HCT-8 cells cultured as previously described. Basal infection was allowed for 2 hours at 37°C. The monolayer was then washed and media replaced with 250 µl of fresh RPMI-1640 with 10% FBS and 1X antibiotic/antimycotic solution. Infected cells were incubated at 37°C for 16 hours (before parasite egress at 19-24 hrs). After incubation, cells were harvested by trypsinization and then washed, fixed, resuspended in 1X PBS and analyzed by flow cytometry.

Merozoite egress assay.

We evaluated the effect of silencing using an egress model by measuring the number of merozoites in supernatants collected between 16-19 hrs post-infection. For these experiments we induced the silencing after infection of the HCT-8 cells. After sporozoite infection of HCT-8 cells, media was removed and cells were transfected with ssRNA/hAgo2 complexes and incubated at 37°C for 16 or 19 hours. RPMI media was removed at 16 hours, replaced with 250 µl of fresh RPMI media, and incubated for 3 hours more to complete the 19 hours incubation period. After incubations, the supernatant was collected, filtered and fixed as before. After the supernatant was removed, the remaining cell monolayer was trypsinized, washed, fixed and filtered. The supernatant and the cells monolayer were separately analyzed by flow cytometry.

Anticryptosporidial activity of ellagic acid on infected cells.

To evaluate anticryptosporidial effect of ellagic acid HCT-8 cells were infected with CFSE-labeled sporozoites. After 1 hour of infection, media was replaced with 250 µl of serum-free RPMI media (free serum) containing varying concentrations of ellagic acid [0, 3, 30, 300 nM and 3µM] and incubated the sample for 16 hrs. After the incubation, the monolayers in the plate were washed with PBS. The cells were trypsinized, fixed and analyzed by flow cytometry as described. For RT-PCR experiments, monolayers were washed with PBS. After removing the supernatant, 350 µl of RLT buffer was added and RNA extracted with RNAeasy kit

Results

Silencing of Actin, Rom1, NDK, and TB2. Four (21nt) ssRNA antisense sequences each were synthesized complementary to mRNA of Actin, Rom1, DKN, and TB2 (Table S2). Complexes for all 4 targeted genes led to >75% decreased expression when compared to controls (unrelated

ssRNA, scramble ssRNA or untreated parasites, (Table 1). ssRNA-Ago did not affect the expression of non-targeted GAPDH mRNA, ribosomal r18s, or parasite viability (Fig. S2).

Silenced targets are not involved on excystation of Cryptosporidium parasites. We evaluated the role of silenced genes during excystation of *Cryptosporidium* sporozoites measuring the excystation rate by fluorescence (Fig 1A). Silencing did not produce a significant reduction on excystation rate for any of the targets (Fig. 1B).

Gene silencing of selected genes blocks parasite entry.

We evaluated gene silencing by flow cytometry using an invasion model (Fig 2A), for these experiments we measured the proportion of CSFE-labeled parasites that failed to invade HCT-8 cells (Fig 2A). First, we defined sporozoites population by flow cytometry (Fig S1A). For the invasion model, we transfected parasites and then evaluated the number of sporozoites in the supernatant s. The results indicates that control group transfected only with PTR has ~65% of stained cells (merozoites), in contrast silencing of Rom1 significantly increased the number of gated cells, meaning that sporozoites did not invaded the host cells (Fig 2B). Silencing of NDK, Ap2 and Actin also showed a partially effect on sporozoite invasion (Fig 2B). We did not observed differences between untreated parasites and transfected parasites with PTR (data not shown).

NDK inhibition reduces parasite proliferation. To evaluate the effects of gene silencing on parasite division we used a proliferation model (Fig 3), parasites were labeled with CFSE and collected at 16 hours post-infection prior to the time of egress (Fig 3). For controls, cell proliferation led to decreased CFSE signal, such that 89% of cells had deceased signal by 16 hours (Fig 3A). By contrast, after silencing of NKD, Ap2 or Actin, only 28-35% of cells had

257 decreased CFSE signal (Figure 3B). Silencing of CP23 and Rom1 had intermediate values,
258 suggesting partial inhibition of proliferation (54-55%). In additional studies we tested the effect of
259 EA acid on sporozoites viability, we did not observe killing effect of EA on sporozoites (Fig S1B).
260
261 ***Silencing of Rom1 and AP2 reduced parasite egress.*** To test the effects of silencing on
262 egress, we transfected intracellular parasites on infected HCT-8 cells. Transfected complexes
263 did not affect the viability of HCT-8 cells (Fig S2), however we observed a reduction on
264 expression in all tested targets (Fig S3). After confirmation of silencing, fresh media was added
265 to collect merozoites released between 16-19 hrs (Fig S4). To evaluate the egress, we
266 conducted qRT-PCR to quantify the relative number of merozoites in supernatants of treated
267 samples and untreated samples (Fig 4B). There was a significant reduction in the number of
268 merozoites observed in the supernatant of silenced samples (Fig 4B). Therefore, these results
269 indicated that silencing of DKN and Actin reduced both parasite proliferation and egress. By
270 contrast, silencing of Ap2 and Rom1 markedly reduced egress out of proportion to the effects on
271 proliferation.
272
273 ***Ellagic acid treatment blocks parasite proliferation.*** Since NDK silencing showed the highest
274 level of reduction in proliferation, we evaluated the anticryptosporidial activity of the NDK
275 inhibitor Ellagic acid (EA) in the HCT-8 infection model. The results showed that EA inhibited
276 parasite proliferation at micromolar concentrations (Fig 5), with an EC50 of within 15-30 μM. In
277 contrast, our results showed that EA is not cytotoxic at these concentrations (Supplementary
278 figure S5). In order to evaluate the anticryptosporidial mechanism, we evaluated the expression
279 of proliferation and apoptosis markers in the parasites. Our results showed a significant down
280 regulation of separine and meta-caspases (Fig 5B-C), which suggest a parasitostatic and
281 parasiticidal effect by blocking proliferation and inducing apoptosis.

Discussion

Cryptosporidium lacks the machinery involved with mammalian gene silencing[6]. In previous studies, we have demonstrated the feasibility to silence *Cryptosporidium* genes by transfecting oocysts with human Argonaute (with slicer activity) loaded with ssRNA[5]. These initial experiments confirmed reduction at protein levels and pointed out the usefulness of the method to evaluate parasite invasion. Since the silencing is maintained up to 24 hrs., then we hypothesized that this method could be used to evaluate other key biological processes during the asexual cycle of parasites maintained in HCT-8 cells (e.g. excystation, proliferation and egress). Thus the overall goal of this study was to use the silencing method to identify targets that are critical for different steps in the parasite life-cycle. Our first step in this work was to identify druggable candidates for gene silencing. We used transcriptional data to prioritize genes highly expressed during invasion, proliferation and egress stages. Also we prioritized genes with low homology with host molecules, but highly conserved between *Cryptosporidium* species. After initial analysis, we identified 100 potential candidates (Fig S1). We developed antisense ssRNA sequences to silence selected genes. In these experiments silencing rates were among 30-94% (Data not shown). Since partial silencing (30-75%) may not be optimal for phenotypic studies, then in this work we only used antisense ssRNA that induces >75%. Selected genes for silencing included: 1) Actin, an structural essential for *Cryptosporidium* motility[7], 2) NDK an essential gene for synthesis of nucleotides [8] 3) Rom1, a protease involved on invasion and egress in other apicomplexan[9] and 4) Ap2, which is a transcription factor involved in proliferation[7]. First, we evaluated the effect of silencing during parasite excystation. The excystation assays showed that none of the silenced genes had effect on this process suggesting that these proteins are not essential for excystation. This result was expected since transcriptomic data has showed that the majority of genes (~85%) in *Cryptosporidium* are expressed after excystation process[10]. The invasion assay indicated that silencing of Rom1

307 blocks parasite entry. This proteolytic enzyme has previously been implicated in parasite
308 invasion[11]. Orthologue rhomboid protease in *Toxoplasma* cleaves cell surface adhesins, and
309 have been demonstrated that this protein is essential for invasion[11]. In *Plasmodium* PfROM1
310 and PfROM4 helped in merozoite invasion by catalyzing the intramembrane cleavage of the
311 merozoite adhesin AMA1[11]. Actin silencing also showed inhibited Invasion. Apicomplexan
312 parasites actively invade host cells using a mechanism predicted to be powered by a parasite
313 actin-dependent myosin motor. Actin in invasion was first suggested by studies demonstrating
314 the ability of the actin polymerization inhibitor cytochalasin D (CytD) to block invasion[12]. The
315 proliferation assay showed that NDK, Ap2, Actin but not Rom1 reduced parasite proliferation.
316 Nucleoside diphosphate kinases (NDK) are enzymes required for the synthesis of nucleoside
317 triphosphates (NTP) other than ATP. They provide NTPs for nucleic acid synthesis, CTP for lipid
318 synthesis, UTP for polysaccharide synthesis and GTP for protein elongation, signal transduction
319 and microtubule polymerization. Not surprisingly, NDK is essential for intracellular parasite
320 proliferation. Actin proteins are related with cytoskeleton motility during cell division.
321 *Cryptosporidium* transcriptomic analysis demonstrated that actin is highly expressed between
322 12-48 hrs after the infection, during this time the parasite is actively dividing passing from a
323 single cell (trophozoite) to 8 cells (meronts II) in 24 hrs. We showed that silencing of AP2
324 transcription factor also affected proliferation (Fig 3B). AP2 proteins are transcription factors
325 which harbor a plant-like DNA-binding domain. Five AP2 proteins have been identified as key
326 stage-specific regulators in *Plasmodium*, thus AP2 proteins have been implicated in *P.*
327 *falciparum* var gene regulation by binding the SPE2 DNA motif and acting as a DNA-tethering
328 protein involved in formation and maintenance of heterochromatin[13]. The role of AP2 proteins in
329 gene regulation has also been investigated to a lesser degree in *T. gondii*, where several AP2
330 proteins have been implicated in regulating progression through the cell cycle [14] as well as
331 crucial virulence factors[15]. Other studies have implicated AP2s in regulating a developmental

transition[16] . Radke et al. [17] recently characterized a *T. gondii* AP2 and showed that this molecule acts as a repressor of bradyzoite development. Our results showed that egress assay was partially affected by parasite proliferation (Fig 4B). Silencing of NDK, AP2 and Actin blocked proliferation leading to a reduction in the number of merozoites (Fig 3B). In contrast, silencing with Rom 1 had an even great effect on egress. Since that protein only had moderate effect in proliferation (Fig 3B), it is likely Rom1 is implicated in parasite egress through a proteolytic mechanism. In *Pla*smodium, release of merozoites from schizonts resulted in the movement of *Plasmodium* ROM1 from the lateral asymmetric localization to the merozoite apical pole and the posterior pole [18].

Overall our in vitro studies confirmed that silenced genes blocks proliferation and egress in *Cryptosporidium* parasites, therefore we hypothesized that chemical inhibitors against these enzymes should arrest *Cryptosporidium* proliferation on infected cells. Since silencing of NDK showed effect during invasion, proliferation and egress then was selected for further studies. The inhibition of NDK activity by EA have been demonstrated [19,20]. Thus here we tested EA on the *Cryptosporidium* infection model, we observed anticryptosporidial activity of this compound at micromolar concentrations (Fig 5A). The EA is a natural compound found in strawberries and other fruits, thus this compound have been used as dietary complement to treat several diseases[21,22], interesting recently this compound showed its antimicrobial activity in the gastrointestinal pathogen *Helicobacter pylori* [23]. In order to investigate the mechanism of anticryptosporidial activity we evaluated expression proliferation (separine) and apoptosis markers (metacaspase) in the parasite. We observed a down regulation in separine expression (also known as separase) which is implicated chromatin regulation during meiosis and mitosis processes[24] , this finding suggest that EA may be blocking proliferation through NDK inhibition as observed in silencing experiments, however also we observed an up regulation of

metacaspase which suggest that other mechanisms may be involved in parasite killing. EA has showed multiple benefits to human health trough enhancement of immune system or epithelial barrier [25-27], thus we speculate that EA has a dual effect on *Cryptosporidium* by reducing the infection trough the activation of host pathways (e.g. defensin secretion) and affecting essential enzymes on parasites. Interesting the micromolar concentrations tested here are under the biological concentration of EA acid commonly used in humans [28], therefore future studies will be focused to characterize the effect of EA and metabolites on intestinal cells of infected mice. If these studies confirm the anticryptosporidial activity and activation of host response then we anticipate that this compound could be implemented in a very near future in the treatment in humans infected with *Cryptosporidium*.

ACKNOWLEDGMENTS

AC was supported by the Bill & Melinda Gates Foundation grant: OPP1161026 and by grant: 5R21AI12627502 from the National Institute of Allergy and Infectious Diseases, National Institutes of Health.

REFERENCES

1 Khalil, I. A. *et al.* Morbidity, mortality, and long-term consequences associated with diarrhoea from Cryptosporidium infection in children younger than 5 years: a meta-analyses study. *Lancet Glob Health* **6**, e758-e768, doi:10.1016/S2214-109X(18)30283-3 (2018).

2 Sparks, H., Nair, G., Castellanos-Gonzalez, A. & White, A. C., Jr. Treatment of Cryptosporidium: What We Know, Gaps, and the Way Forward. *Curr Trop Med Rep* **2**, 181-187, doi:10.1007/s40475-015-0056-9 (2015).

3 Huston, C. D. *et al.* A Proposed Target Product Profile and Developmental Cascade for New Cryptosporidiosis Treatments. *PLoS Negl Trop Dis* **9**, e0003987, doi:10.1371/journal.pntd.0003987 (2015).

4 Checkley, W. *et al.* A review of the global burden, novel diagnostics, therapeutics, and vaccine targets for cryptosporidium. *Lancet Infect Dis* **15**, 85-94, doi:10.1016/S1473-3099(14)70772-8 (2015).

5 Castellanos-Gonzalez, A., Perry, N., Nava, S. & White, A. C., Jr. Preassembled Single-Stranded RNA-Argonaute Complexes: A Novel Method to Silence Genes in Cryptosporidium. *The Journal of infectious diseases* **213**, 1307-1314, doi:10.1093/infdis/jiv588 (2016).

6 Abrahamsen, M. S. *et al.* Complete genome sequence of the apicomplexan, Cryptosporidium parvum. *Science* **304**, 441-445, doi:10.1126/science.1094786 (2004).

7 Wetzel, D. M., Schmidt, J., Kuhlenschmidt, M. S., Dubey, J. P. & Sibley, L. D. Gliding motility leads to active cellular invasion by Cryptosporidium parvum sporozoites. *Infection and immunity* **73**, 5379-5387, doi:10.1128/IAI.73.9.5379-5387.2005 (2005).

8 Weiss, B. The deoxycytidine pathway for thymidylate synthesis in Escherichia coli. *J Bacteriol* **189**, 7922-7926, doi:10.1128/JB.00461-07 (2007).

9 Sibley, L. D. How apicomplexan parasites move in and out of cells. *Curr Opin Biotechnol* **21**, 592-598, doi:10.1016/j.copbio.2010.05.009 (2010).

10 Mauzy, M. J., Enomoto, S., Lancto, C. A., Abrahamsen, M. S. & Rutherford, M. S. The Cryptosporidium parvum transcriptome during in vitro development. *PloS one* **7**, e31715, doi:10.1371/journal.pone.0031715 (2012).

11 Zhao, H. F. *et al.* High-throughput screening of effective siRNAs from RNAi libraries delivered via bacterial invasion. *Nat Methods* **2**, 967-973, doi:10.1038/nmeth812 (2005).

12 Dobrowolski, J. M. & Sibley, L. D. Toxoplasma invasion of mammalian cells is powered by the actin cytoskeleton of the parasite. *Cell* **84**, 933-939 (1996).

13 Flueck, C. *et al.* A major role for the Plasmodium falciparum ApiAP2 protein PfSIP2 in chromosome end biology. *PLoS pathogens* **6**, e1000784, doi:10.1371/journal.ppat.1000784 (2010).

14 Radke, J. B. *et al.* ApiAP2 transcription factor restricts development of the Toxoplasma tissue cyst. *Proceedings of the National Academy of Sciences of the United States of America* **110**, 6871-6876, doi:10.1073/pnas.1300059110 (2013).

15 Lesage, K. M. *et al.* Cooperative binding of ApiAP2 transcription factors is crucial for the expression of virulence genes in Toxoplasma gondii. *Nucleic acids research* **46**, 6057-6068, doi:10.1093/nar/gky373 (2018).

16 Huang, S. *et al.* Toxoplasma gondii AP2IX-4 Regulates Gene Expression during Bradyzoite Development. *mSphere* **2**, doi:10.1128/mSphere.00054-17 (2017).

17 Radke, J. B. *et al.* Transcriptional repression by ApiAP2 factors is central to chronic toxoplasmosis. *PLoS pathogens* **14**, e1007035, doi:10.1371/journal.ppat.1007035 (2018).

18 Singh, S., Plassmeyer, M., Gaur, D. & Miller, L. H. Mononeme: a new secretory organelle in Plasmodium falciparum merozoites identified by localization of rhomboid-1 protease. *Proceedings of the National Academy of Sciences of the United States of America* **104**, 20043-20048, doi:10.1073/pnas.0709999104 (2007).

19 Buxton, I. L. Inhibition of Nm23H2 gene product (NDPK-B) by angiostatin, polyphenols and nucleoside analogs. *Proc West Pharmacol Soc* **51**, 30-34 (2008).

20 Malmquist, N. A., Anzinger, J. J., Hirzel, D. & Buxton, I. L. Ellagic acid inhibits nucleoside diphosphate kinase-B activity. *Proc West Pharmacol Soc* **44**, 57-59 (2001).

21 Soh, P. N. *et al.* In vitro and in vivo properties of ellagic acid in malaria treatment. *Antimicrobial agents and chemotherapy* **53**, 1100-1106, doi:10.1128/AAC.01175-08 (2009).

22 Ceci, C. *et al.* Experimental Evidence of the Antitumor, Antimetastatic and Antiangiogenic Activity of Ellagic Acid. *Nutrients* **10**, doi:10.3390/nu10111756 (2018).

23 De, R. *et al.* Antimicrobial activity of ellagic acid against Helicobacter pylori isolates from India and during infections in mice. *J Antimicrob Chemother* **73**, 1595-1603, doi:10.1093/jac/dky079 (2018).

24 Gurvits, N. *et al.* Separase is a marker for prognosis and mitotic activity in breast cancer. *Br J Cancer* **117**, 1383-1391, doi:10.1038/bjc.2017.301 (2017).

25 Promsong, A., Chung, W. O., Satthakarn, S. & Nittayananta, W. Ellagic acid modulates the expression of oral innate immune mediators: potential role in mucosal protection. *J Oral Pathol Med* **44**, 214-221, doi:10.1111/jop.12223 (2015).

26 Marin, M., Maria Giner, R., Rios, J. L. & Recio, M. C. Intestinal anti-inflammatory activity of ellagic acid in the acute and chronic dextrane sulfate sodium models of mice colitis. *J Ethnopharmacol* **150**, 925-934, doi:10.1016/j.jep.2013.09.030 (2013).

27 Goyal, Y., Koul, A. & Ranawat, P. Ellagic acid ameliorates cisplatin induced hepatotoxicity in colon carcinogenesis. *Environ Toxicol*, doi:10.1002/tox.22747 (2019).

28 Liu, Y. *et al.* Chronic administration of ellagic acid improved the cognition in middle-aged overweight men. *Appl Physiol Nutr Metab* **43**, 266-273, doi:10.1139/apnm-2017-0583 (2018).

Supporting Information Legends

Table and Figures Legends (supplemental data)

Table S1. Accession numbers of *Cryptosporidium* sequences used for antisense ssRNA design.

Table S2. *Cryptosporidium* antisense ssRNA sequences used in this study.

464 Table S3. Target genes and primer sequences used for RT-PCR analysis.

465

466 Figure S1. Sporozoites of *Cryptosporidium* by Flow cytometry (A). Cryptosporidium oocysts
467 were stained with CFSE and then excystation was induced. Parasites were filtered and then
468 sample was analyzed by flow cytometry. Effect of EA on oocyst and excystation by flow
469 cytometry (B), we treated stained oocyst with EA and then excystation was induced.

470

471 Figure S2. Expression of human 18s gene in HCT-8-cells after transfection. HCT-8 cells were
472 infected with *Cryptosporidium* sporozoites and then transfected with ssRNA. For these
473 experiments, after 2 hours of infection the supernatant was removed and new culture media
474 was added. Next, silencer complexes were added to the infected cells and incubated overnight.
475 To evaluate cytotoxic effects of ssRNA or HCT-8 we quantified 18s rRNA, if cells die this should
476 be reflected as reduction of this marker. Figure shows no differences between wild type (WT),
477 protein transfection reagent alone (PTR), and tested ssRNAs ssAct, ssAp2, ssNDK, ssRom1
478 (encapsulated in PTR).

479

480 Figure S3. Gene silencing after infection. In this experiment we tested the silencing on
481 intracellular forms (merozoites) within HCT-8 cells. For these experiments we infected and
482 treated cells as described above and we evaluated the silencing by qRT-PCR in total RNA from
483 infected cells transfected with silencer complexes. The figure shows PCR CT values from
484 duplicate experiments of transfected cells with silencer complexes (gray bar) and cells
485 transfected only with PTR. All cells treated with ssRNA showed a delay in the amplification cycle
486 when compared with controls. All samples were normalized against GAPDH. Standard deviation
487 of PCR triplicates is shown in each bar.

488

Figure S4. *Cryptosporidium* merozoites collected at 16 hrs of infection. *Cryptosporidium* merozoites by flow cytometry. HCT-8 cells were infected with labeled sporozoites. After infection, silencing was induced, then at 16 hrs of infection (before egress) supernatant was removed and fresh media was added. Supernatant was collected again a 19 hrs and analyzed by flow cytometry, then % of merozoites were evaluated in samples treated only with PTR (left), merozoites are not observed in supernatants of non-infected samples (right).

Figure S5. Ellagic acid and viability on HCT-8 cells. Effect of EA on non-infected (NI) HCT-8 cells. HCT-8 cells were treated with EA (or not) and then viability was evaluated measuring the activation of the vital dye CFSE. The figure shows the % of cells positives for CFSE.

Table and Figures Legends (main manuscript)

Table 1. Gene silencing in *Cryptosporidium*. Selected targets (yellow column) were silenced with antisense ssRNA (gray column) and hAgo2 complexes. Silencing was evaluated by RT-PCR and Ct values were determined in treated with hAgo2/target ssRNA (red column) and hAgo2/unrelated ssRNA (green column). The silencing was calculated as fold change relative to control sample and expressed as percentage, SD=standard deviation (blue column).

Figure 1. *Cryptosporidium* excystation assay. *Excystation model (A).* Parasites were stained with a vital dye (highlighted in green) and transfected with hAgo2/target ssRNA (highlighted in yellow), then excystation was induced and sporozoites were filtered (highlighted in blue). Sporozoites were quantified by fluorometry (highlighted in purple). *Effect of silencing on excystation (B). Cryptosporidium* oocysts were transfected with silencer complexes (+) or not (-), we induced excystation and compared fluorescence in treated (grey bars) and untreated

514 oocysts (black bar). Experiments were conducted by triplicate. Non statistical difference was
515 observed between control and treated samples.
516
517 Figure 2. *Cryptosporidium* invasion assay. *Invasion model (A).*Transfected parasites were used
518 to infect HCT-8 cells (infected cells shown in red square), after 1 hr of infection supernatant
519 (square green) was collected and % of sporozoites was evaluated by flow cytometry. *Effect of*
520 *silencing on parasite entrance by Flow cytometry (B).* Silencing was induced or not (PTR) and
521 then sporozoites were used to infect cells, parasites that did not invade cells were evaluated in
522 supernatants (SN). wt= unstained wild typte, PTR= parasites treated only with protein
523 transfection reagent.
524
525 Figure 3. *Cryptosporidium* proliferation assay. Stained parasites (sowed in green) were
526 transfected and then used to infect HCT-8 cells, division of WT parasites within infected cells
527 was analyzed by flow cytometry 0-16 hrs tracking reduction of fluorescent signal (A). Division of
528 transfected parasites was analyzed at 16 hrs and compared with untreated parasites (PTR) or
529 parasites treated with unrelated target Cp23 (B).
530
531 Figure 4. *Cryptosporidium* egress assay. Egress model (A). Parasites were stained (green) and
532 used to infect HCT-8 cells. We induce silencing on parasites within infected cells. Then,
533 supernatant from 16-19 hrs was collected and evaluated by flow cytometry (B). Total numbers
534 of parasites (in 200 µl) were determined by qRT-PCR in treated samples (grey bars) and control
535 sample treated only with PTR (red bar) and non-infected cells (NI). The experiments were
536 conducted in triplicates, SD and p values (*= $p \leq 0.05$) are shown.
537

538 Figure 5. Anticryptosporidial activity of Ellagic acid (EA). Reduction of parasites on infected cells
539 by EA. We infected human intestinal cells (HCT-8) with *Cryptosporidium*, after the infection cells
540 were treated with different amounts of EA and then we evaluated the parasite burden by qRT-
541 PCR (A). Activation of apoptosis by EA. We evaluated expression of apoptosis marker
542 metacaspase in treated (with bar) and untreated (grey bar) cells (B). Inhibition of proliferation by
543 EA. Expression of proliferation marker separine was evaluated by qRT-PCR on infected cells
544 treated (with bar) and untreated (grey bar) with EA (C). RT-PCR experiments were conducted
545 by triplicate, and standard deviation is indicated in each bar.

Table 1

RT-PCR amplified Target	Antisense ssRNA 21nt	Ct value Ago/ssRNA	Ct value Ago/unrelated RNA	% silencing ± SD
Actin	ssAct	31.4 ± 0.4	28.3 ± 0.8	78 ± 3
Ago2	ssAgo2	25.3 ± 0.3	21.3 ± 0.2	94 ± 0
NDK	ssNDK	27.3 ± 0.7	23.6 ± 0.6	93 ± 0
Rom1	ssRom1	46.5 ± 4.1	43.0 ± 2.7	96 ± 1

Figure 1

A

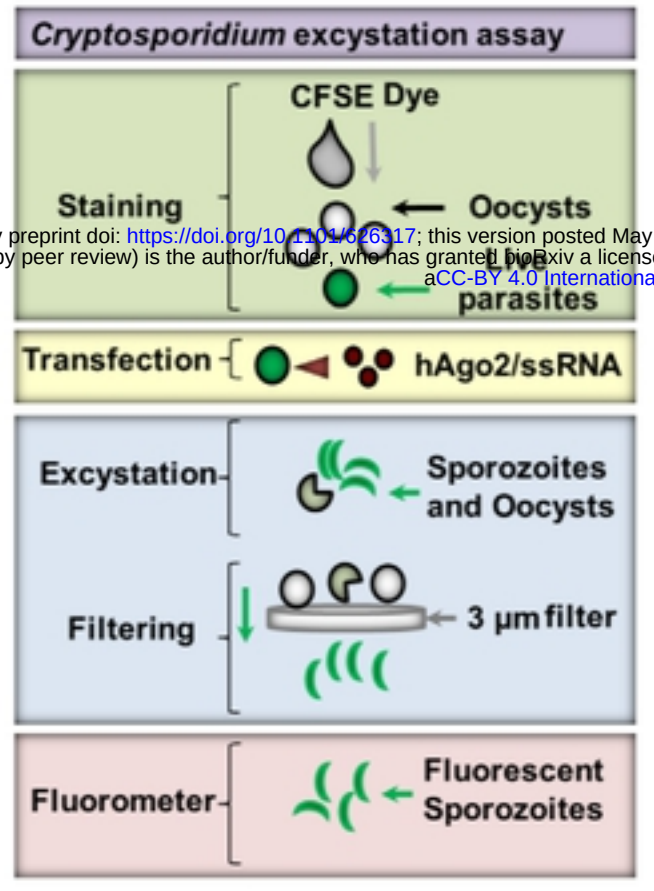

B

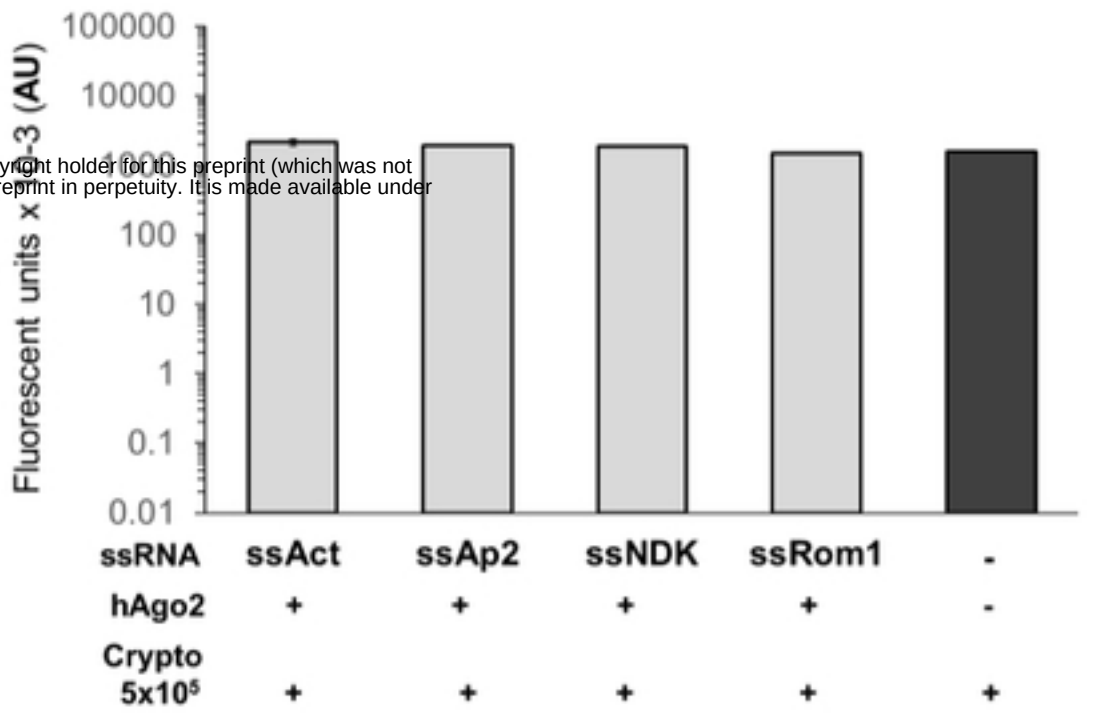

Figure 2

A

B

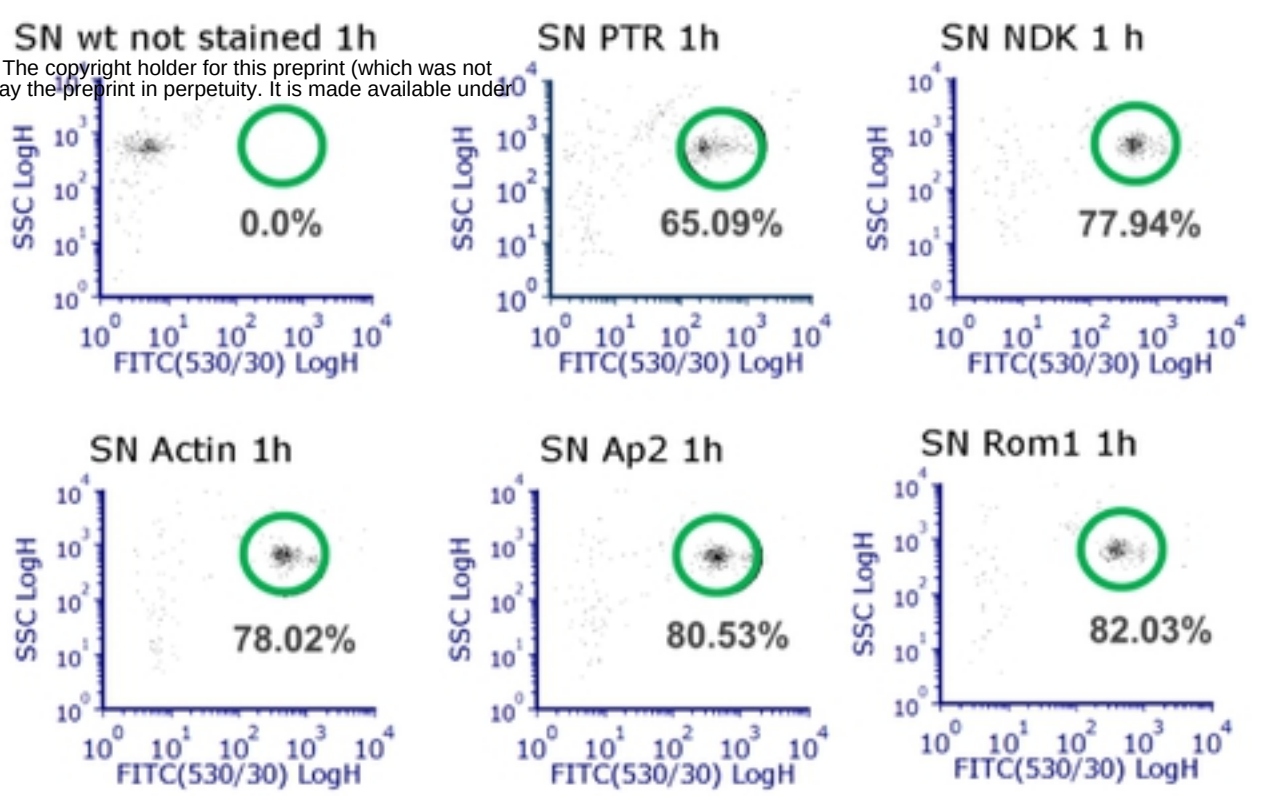

Figure 3

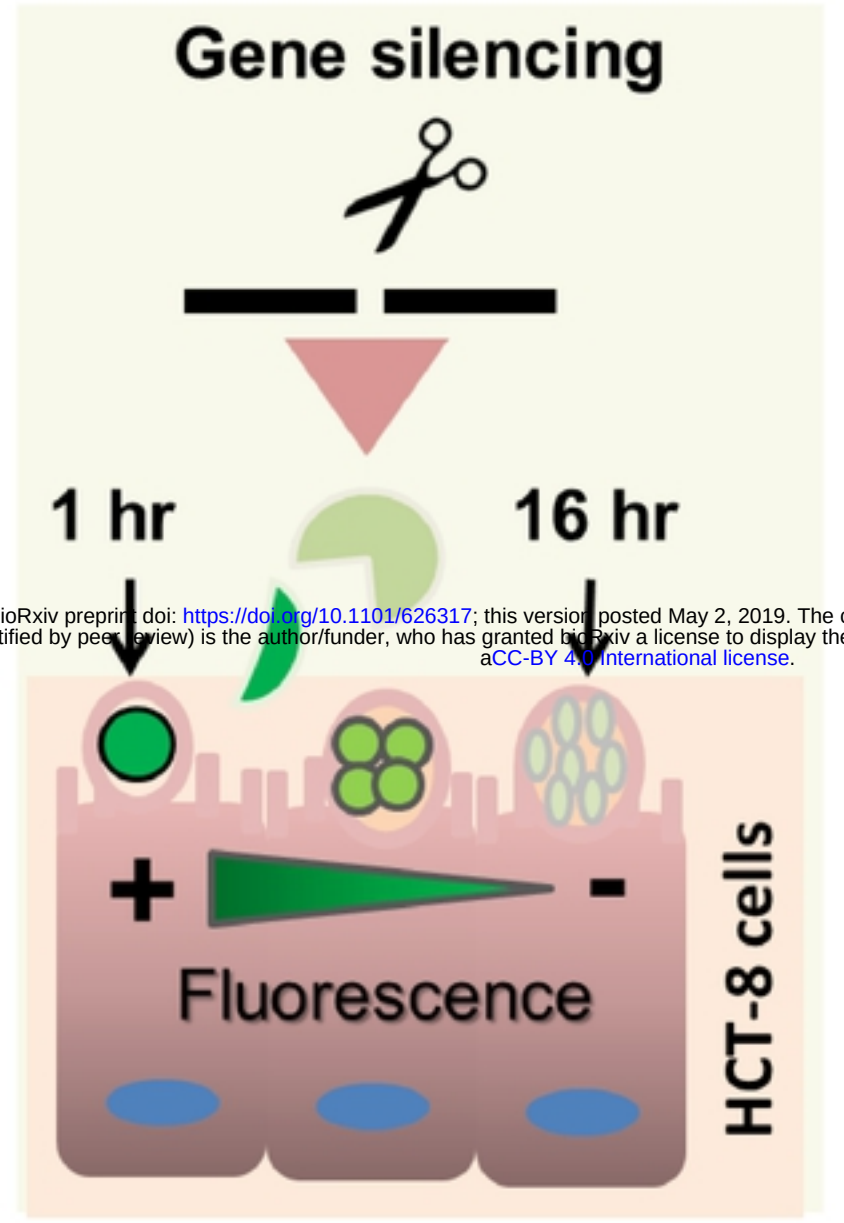

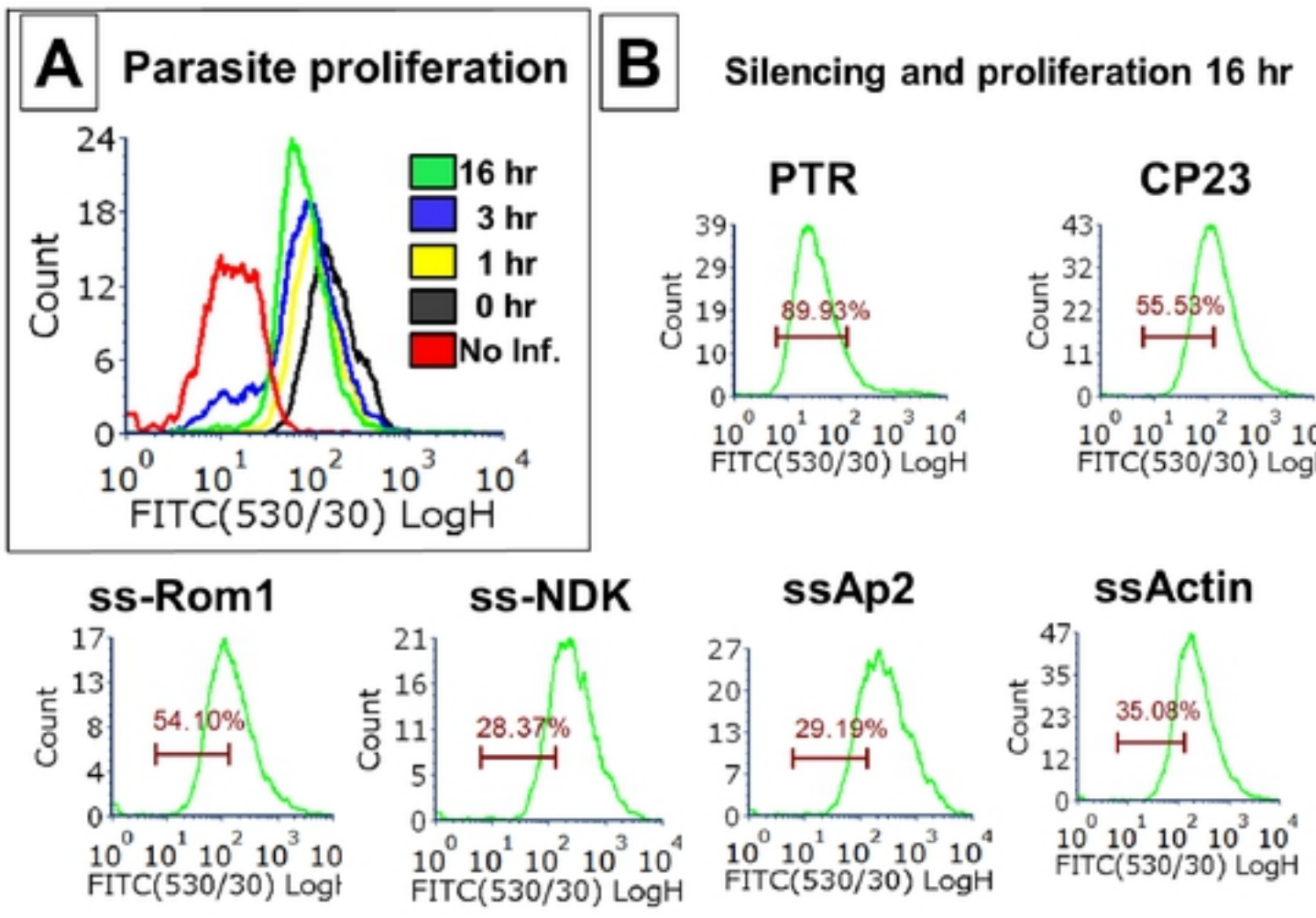

Figure 4

A

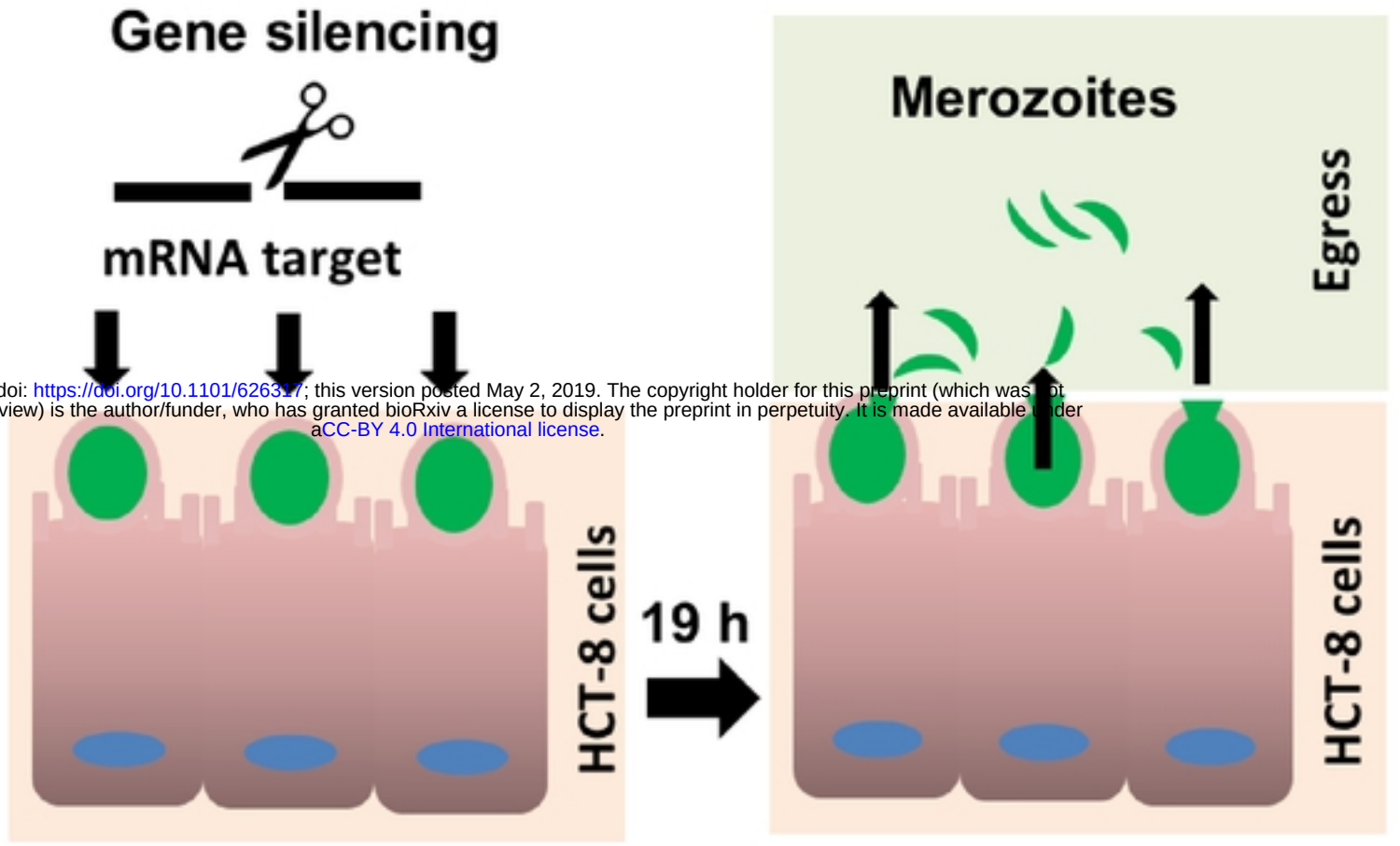

B

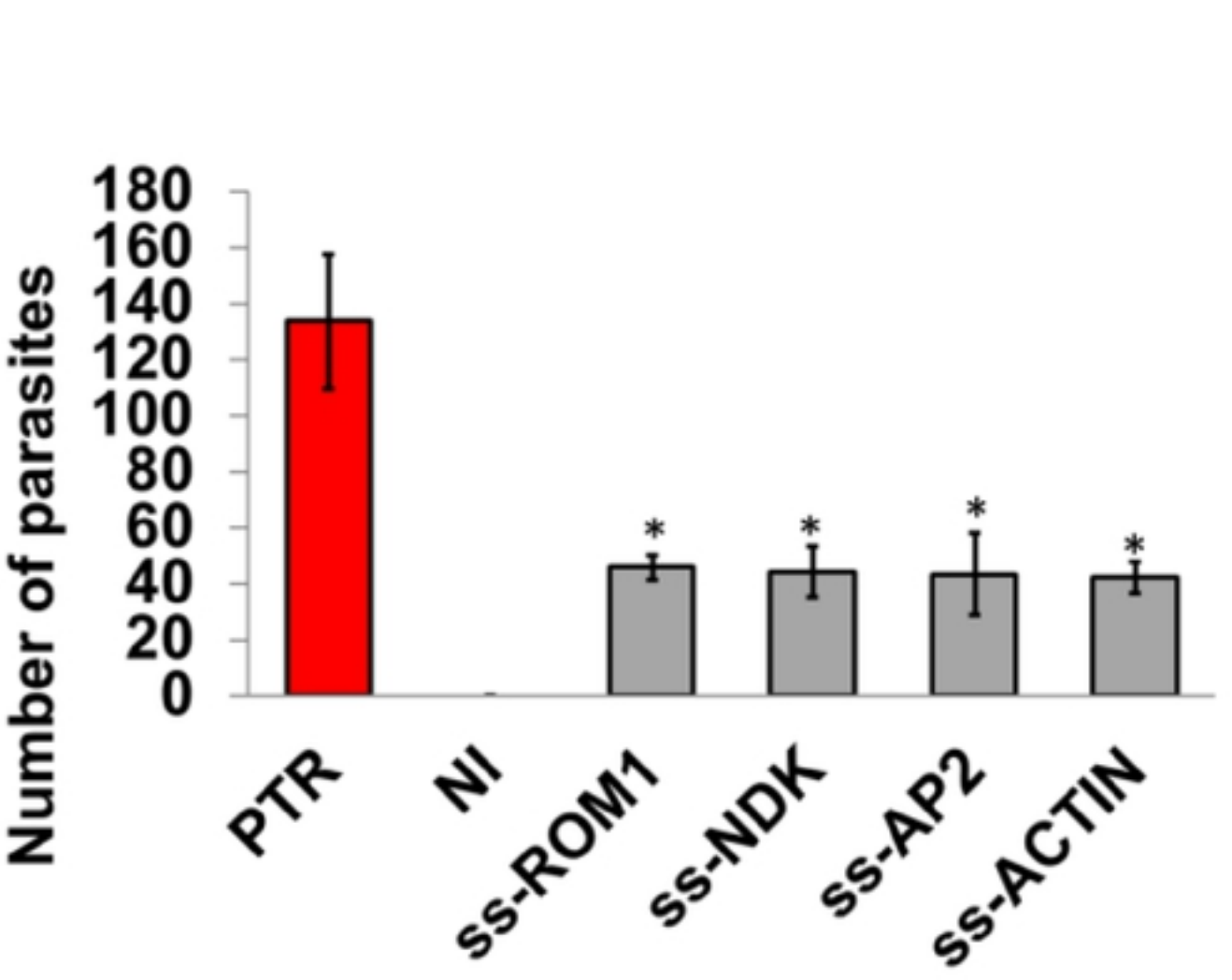

Figure 5

A

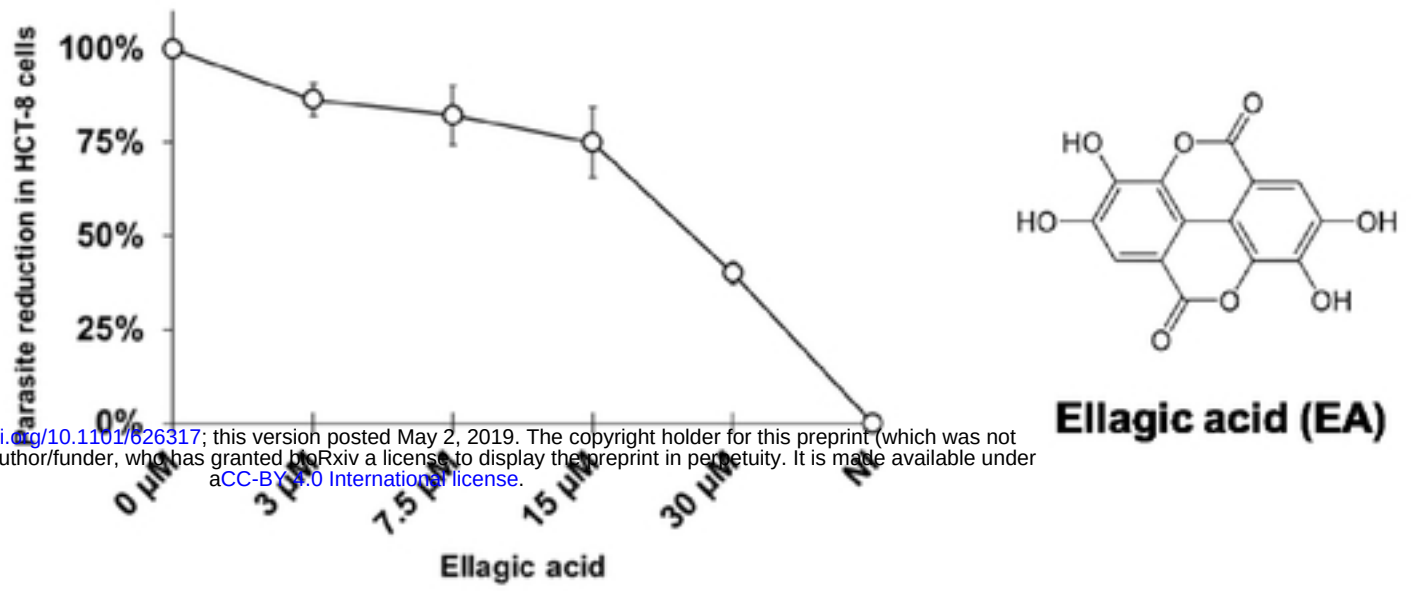

B

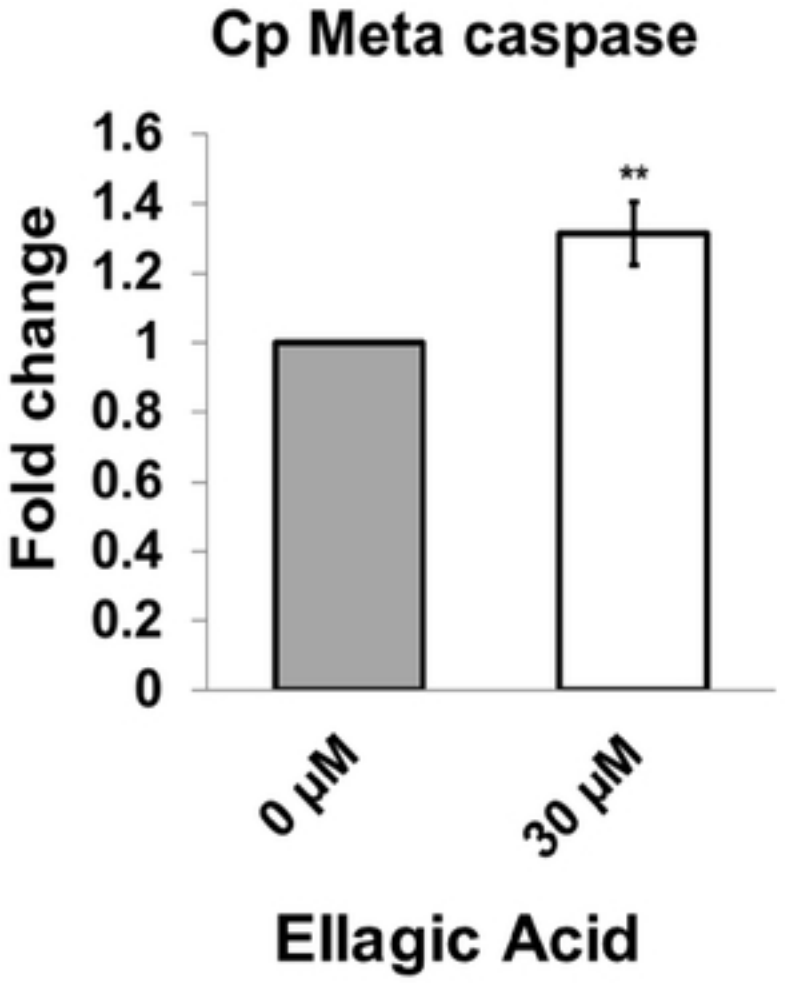

C